EVALUATION OF AN ELECTRIC TURBO COMPOUND SYSTEM FOR SI ENGINES: A NUMERICAL APPROACH

Gianluca Pasini[a], **Giovanni Lutzemberger**[a], **Stefano Frigo**[a], **Silvia Marelli**[b], **Massimo Ceraolo**[a], **Roberto Gentili**[a], **Massimo Capobianco**[b]

a)   University of Pisa - DESTEC
      Largo Lucio Lazzarino
      56122 Pisa (ITALY)
      Tel.   +39-050-2217100
      Fax   +39-050-2217150

b)   University of Genoa - DIME
      Via Montallegro, 1
      16145 Genoa (ITALY)
      Tel.   +39-010-3532443
      Fax   +39-010-3532566

Corresponding Authors:

Gianluca Pasini
Department of Energy, System, Territory
and Construction Engineering (DESTEC)
University of Pisa
Largo Lucio Lazzarino
56122 Pisa (ITALY)
Tel.   +39-050-2217161
Fax   +39-050-2217150
Email gianluca.pasini@for.unipi.it

32 **ABSTRACT**

33 In a medium term scenario hybrid powertrain and Internal Combustion Engine (ICE) downsizing
34 represent the actual trend in vehicle technology to reduce fuel consumption and CO_2 emission.
35 Concerning downsizing concept, to maintain a reasonable power level in small engines, the
36 application of turbocharging is mandatory both for spark ignition (SI) and compression ignition (CI)
37 engines. Following this aspect, the possibility to couple an electric drive to the turbocharger
38 (electric turbo compound) to recover the residual energy of the exhaust gases is becoming more
39 and more attractive, as demonstrated by several studies around the world and by the current
40 application in the F1 Championship.

41 The present paper shows the first numerical results of a research program under way in
42 collaboration between the Universities of Pisa and Genoa. This first study is focused on the
43 evaluation of the benefits resulting from the application of an ETC to a small twin-cylinder SI
44 engine (900 cm^3). Starting from the experimental maps of two turbines and one compressor, the
45 complete model of a turbocharged engine was created using the AVL BOOST one-dimension
46 code. The numerical activity then moves to the whole vehicle/powertrain modelling, considering
47 three driving cycles and two different vehicle configurations, in order to verify the effectiveness of
48 the proposed ETC solution.

49 Results show that ETC is not beneficial over a conventional turbocharger with appropriate turbine
50 geometry if the target is to optimize the overall efficiency in one specific operating point of the ICE,
51 like in the case of range-extended electric vehicles. Besides, ETC can slightly improve the average
52 overall efficiency when the ICE must provide variable power output, as in the case of conventional
53 or hybrid vehicles. However, the major benefits coming from ETC are the boost range extension in
54 the lowest engine rotational speed region and a possible reduction of turbo lag, which are key
55 points in parallel-hybrid and especially in conventional vehicles.

56 Concerning the whole vehicle/powertrain simulation, first results show that the ETC does not
57 improve fuel economy of the smaller vehicle, especially when employed in urban cycles. The ETC
58 is much more advantageous in the case of the larger vehicle, particularly when extra-urban roads
59 or motorways are considered.

60

61

62 KEYWORDS – Internal Combustion Engines, Exhaust gas energy recovery, Turbocharger
63 flow maps, Electric Turbo Compound, Hybrid Vehicle, Electric Vehicle.

64

65

NOMENCLATURE AND DEFINITIONS

CA   Crank Angle
CADC   Common Artemis Driving Cycle
BSFC   Brake Specific Fuel Consumption
CI   Compression Ignited
ICE   Internal Combustion Engine
imep   indicated mean effective pressure
NEDC   New European Driving Cycle
rpm   revolution per minute
SI   Spark Ignited
SOC   State of charge
TC   Turbocharger

Notation:

n	rotational speed	rpm
p	pressure	bar
A	waste-gate opening degree	%
M	mass flow rate	kg/s
N	rotational speed factor	rpm/$\sqrt{K}$
T	temperature	K
β	compression ratio	
ε	expansion ratio	
η	efficiency	
Φ	mass flow rate factor	kg·$\sqrt{K}$/(s·bar)

Subscripts:

0	reference condition
1	compressor inlet section
2	compressor exit section
3	turbine inlet section
4	turbine exit section
c	compressor
r	reduced
s	isentropic
t	turbine
S	static condition
T	stagnation condition

1. Introduction

With growing concern for environmental problems, in the last years more stringent standards for vehicle fuel consumption and emissions have been introduced. Therefore, vehicle manufacturers focused their attention on the development of modified conventional vehicles in hybrid versions. These vehicles have advanced powertrains for efficient utilization of energy, in order to recover energy during braking and allow the Internal Combustion Engine (ICE) to operate on its highest efficiency region. Additionally, depending on the hybrid powertrain typology (i.e. series hybrid, parallel hybrid, range extended, etc.), the ICE can also be significantly downsized.

In this regard, to maintain a reasonable power level in small ICEs, the application of turbocharging (TC) technology is mandatory, both for spark ignited (SI) and compression ignited (CI) engines. To this aim, the possibility to couple an electric drive to the turbocharger (Electric Turbo Compound, ETC) to recover the residual energy of the exhaust gas, as well as to extend the boost range and reduce the turbo lag, is becoming more and more attractive, as demonstrated by several studies around the world and by the current application in the F1 Championship.

This approach belongs to a wider topic, which is the maximum recovery of the residual energy from the exhaust gas to regenerate it either within the engine crankshaft or within auxiliary powertrain units inside the vehicle. Without entering into details, which are well explained in the recent open literature [1÷3], it is meaningful to outline that, at present, three main technologies are being studied for exhaust energy recovery in the automotive sector, i.e., ORCs (Organic Rankine Cycles), thermoelectric generators and turbo compounding.

The Organic Rankine Cycles offer waste heat recovery without imposing any additional backpressure to the engine as it does not restrict the exhaust gas flow leaving the engine. Despite a potential improvement in BSFC (Brake Specific Fuel Consumption) of as much as 15%, the implementation of ORCs requires a complex engineering architecture, which makes it not suitable for small-scale applications such as passenger vehicles [4-10].

Similarly, thermoelectric generators do not increase exhaust back-pressure. The principle of thermoelectric generation relies on the Peltier-Seebeck effect which accounts for the direct conversion of thermal energy into electric energy. Nevertheless, the efficiency of electric conversion is poor and requires large surface areas which are not always available in automotive applications. Besides, the cost of the material for thermoelectric generator devices is still high, thus this technology is not yet practical for commercialisation [11÷15].

The last method to recover exhaust gas energy from ICEs is represented by the adoption of turbocompounding technology. Turbocompounding consists in the addition of a mechanic or electric device to the main turbocharger turbine in order to recover the excess of energy available in the exhaust.

Mechanical turbocompounding technology [16÷19] involves the installation of a power turbine besides the Turbocharger (TC) turbine for extracting mechanical power from the exhaust gas stream. Mechanical turbocompounding is well known for being used on aircraft engines in the 1950's. The three most successful and documented engines are the Wright R-3350, the Napier Nomad and the Allison V-1710. Today, mechanical turbocompounding is mainly used on large displacement diesel engines designed for use in heavy ground vehicles such as trucks and agricultural equipment adopted, for example, by Scania, Volvo and Detroit Diesel.

149 The electrical turbocompounding strategy is based on two configurations: in the first layout an
150 additional turbine is placed on the exhaust line, usually downstream of the turbocharger turbine,
151 linked to a small electric generator (turbo generator) [20÷22]. The second configuration is based on
152 coupling an electrical generator to the TC shaft for extracting excess power produced by the
153 turbine (electric turbo compound) [23÷28]. In this case, the turbine produces more power than the
154 necessary to drive the compressor. The excess power is converted into electric power using a high
155 speed generator incorporated in the TC casing. The electrical drive can be also used to accelerate
156 the TC shaft and reduce the turbo lag, despite the overall increased inertia. An alternative solution
157 is the use of a turbine and a compressor without mechanical link, both with individual electric drive.

158 In the present paper, the first numerical results of a joint research program developed by the
159 Universities of Pisa and Genoa are shown. Very few papers present studies related to the
160 application of an ETC to SI engines [28, 29] and no one has been made adopting the numerical
161 codes here applied.

162 In the first part of the study, the evaluation of the benefits resulting from the application of an ETC
163 to a small-size twin-cylinder S.I. engine has been examined. In particular, utilizing the AVL
164 BOOST-1D computational program, implemented with experimental turbocharger characteristic
165 curves, an estimation of the global amount of the energy recovered from exhausts is predicted,
166 providing further insights into engine operating range where ETC is beneficial with respect to a
167 conventional TC and giving hints on how to size the turbine geometry to maximize the recovered
168 energy. Concerning this last aspect, some Authors noted the importance of choosing a power
169 turbine flow capacity large enough to avoid high backpressure penalties, even if slight or no effect
170 on fuel consumption occurs [29].

171 In the second part of the study, the numerical activity moves to the whole vehicle/powertrain
172 modelling adopting the 3DS's Dymola code based on Modelica language. Engine results are
173 utilized to identify the optimal way to exploit the electrical energy recovered. Vehicle powertrain
174 architecture of a conventional vehicle equipped with a standard TC group is kept unmodified as
175 much as possible, as well as that of the electrical system, apart the introduction of the ETC device.
176 Three driving cycles and two different vehicle configurations have been analysed. The three driving
177 cycles, all from CADC (Common Artemis Driving Cycle), are able to represent the vehicle usage in
178 urban, extra-urban roads and motorways in a realistic way.

179

180 ## 2. Experimental results on turbocharger performance

181 Turbine and compressor maps implemented in the engine simulation model are properly selected
182 referring to an experimental database available at the Internal Combustion Engines Group (ICEG)
183 of the University of Genoa. In particular, two turbines and one compressor are identified. Both
184 turbines are single entry nozzleless radial flow units, fitted with a waste-gate valve. The first turbine
185 (Garrett GT2052, called A) is characterized by 47 mm rotor diameter and by a $TRIM_t$ level equal to
186 0.72, the second (IHI RHF3, called B) by a rotor diameter of 33 mm and by a $TRIM_t$ equal to 0.81.
187 Selected compressor is a radial flow type (IHI RHF3) characterized by an impeller diameter of
188 about 40 mm.

189 Experimental characteristic curves of the turbomachines have been measured at the turbocharger
190 test facility of the University of Genoa (Figure Fig. 1), fully described in previous papers [30, 31, 32].
191 The compressed air apparatus is fitted with three electrical screw compressors able to provide a
192 total mass flow rate of about 0.6 kg/s at a maximum pressure of 8 bar. An electric heater allows

193 increasing turbine inlet temperature up to 750 °C. However, turbine experimental maps here
194 selected refer to an inlet air temperature of about 80 °C ("cold operation").

195 Even if experimental results here reported refer to turbine and compressor steady flow
196 characteristic curves, it must be mentioned that the possibility to reproduce the unsteady flow
197 typically occurring in the intake and exhaust engine circuit is a peculiarity of the UNIGE test facility.
198 In particular, two different arrangements respectively using diametral slot rotating valves or a motor
199 driven cylinder head are available, fully described in [30, 33].

200 Measurements are performed by an automatic data acquisition system, using interactive
201 procedures in LabVIEW® environment. All quantities here reported are an ensemble average of
202 multiple data acquisition (10 cycles). Therefore, measurements are referred to the average level of
203 data recorded at the same operating condition. Under steady flow condition, static pressure levels
204 are measured at the inlet and outlet section of compressor and turbine through strain-gauge
205 transducers characterized by an accuracy of ±0.15% of the full scale. A high frequency response
206 piezoresistive pressure sensor mounted just downstream of the compressor volute exit is used to
207 measure instantaneous pressure signal to detect surge phenomenon [30]. Total air temperature
208 levels are measured through platinum resistance thermometers (Pt 100 Ohm) with a measurement
209 tolerance of ±0.15 °C + 0.2% of measured value. All sensors are crosswise inserted in the flow
210 pipe. With particular reference to the compressor outlet section, three different probes are
211 generally adopted to evaluate compressor efficiency (therefore turbine thermo-mechanical
212 efficiency) with good accuracy. Turbocharger rotational speed is measured by an inductive probe
213 mounted close to the compressor wheel allowing to detect rotor revolution with good accuracy.
214 Compressor mass flow rate is measured through a thermal mass flow meter with a measurement
215 tolerance of ±0.9% of measured value and ±0.05% of the full scale. As regards turbine mass flow
216 rate, this quantity is measured through a laminar flow meter (measurement tolerance of ±2% of
217 measured value).

218 In Figure 2 steady flow characteristic curves of both considered turbines measured at different
219 levels of rotational speed factor ranging from 2000 to 7000 rpm/√K are shown. Turbine maps are
220 referred to the complete closure of the by-pass system (waste-gate valve), since only turbine maps
221 with the regulating device fully closed are implemented in the simulation model. Since results here
222 reported are measured in "cold conditions", all quantities are scaled based on the conventional
223 non-dimensional groups to properly take into account for the density variation of the flow entering
224 the turbine.

225 Turbine maps are then referred to the following parameters:

226 - turbine rotational speed factor: [rpm/√K]
227

$$N_t = \frac{n}{\sqrt{T_{T3}}}$$

228

229

230 - Expansion ratio (total-to-static): [-]
231

$$\varepsilon_{TS} = \frac{p_{T3}}{p_{S4}}$$

232

233

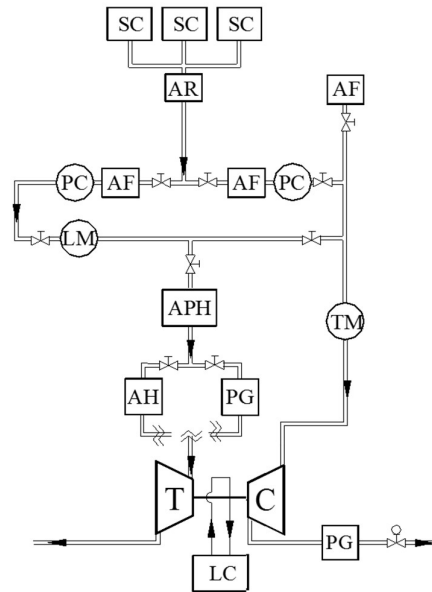234   -   Mass flow rate factor: [kg·√K/(s·bar)]

235

$$\Phi_t = \frac{M_t \cdot \sqrt{T_{T3}}}{p_{T3}}$$

236

237

238

239

AF	Air Filter	LM	Laminar Flow Meter
AH	Air Heater	PC	Pressure Control
APH	Air Pre-Heater	PG	Pulse Generator
AR	Air Reservoir	SC	Screw Compressor
C	Compressor	T	Turbine
LC	Lubricating Circuit	TM	Thermal Mass Flow Meter

240

241   **Fig. 1: Turbocharger test facility of University of Genoa.**

242

243 In order to measure turbine characteristic curves over an extended range while keeping the
244 turbocharger compressor coupled, modulation of compressor inlet pressure is performed, thus
245 controlling its power absorption, working at higher and lower level than the ambient condition. In
246 Figure 2 it is highlighted that mass flow rate factor is more sensitive to the expansion ratio than to
247 turbine rotational speed at constant waste-gate valve setting. It is worth noticing the extension of
248 each constant speed curve that was achieved at low turbine inlet temperature (about 400 K). The
249 definition of steady flow curves in a wide operating range is an essential requisite to reduce
250 inaccuracies in the extrapolation method adopted within simulation models.
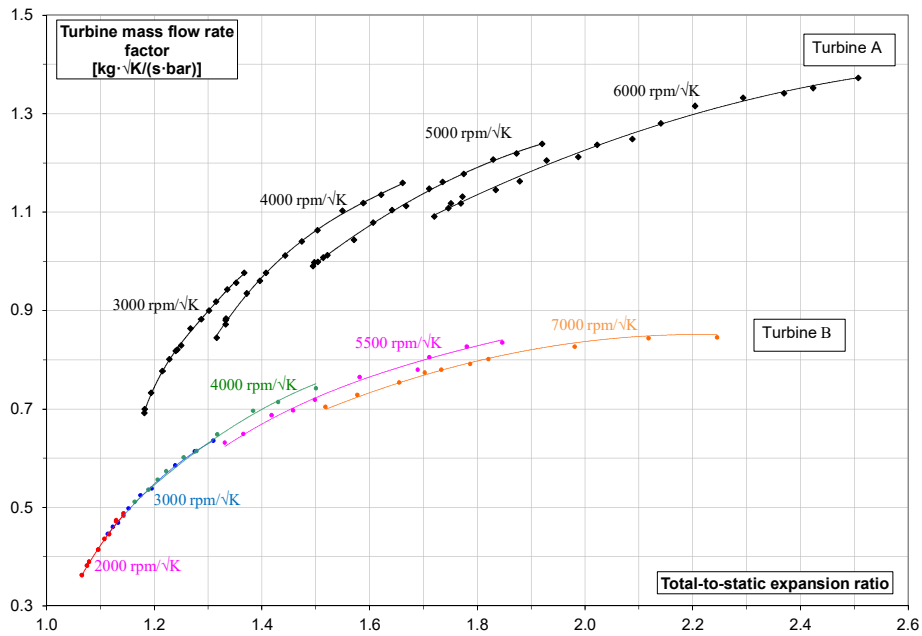
Fig. 2: Measured turbine steady flow maps.

As aforementioned, the compressor selected for this application is characterized by an impeller diameter of about 40 mm is. In Figure 3 total-to-total pressure ratio and total-to-total efficiency vs. corrected mass flow rate are reported referring to different levels of compressor corrected rotational speed.

Compressor maps reported are referred to the following parameters:

- Reduced rotational speed: [rpm]

$$n_{cr} = \frac{n \cdot \sqrt{T_0}}{\sqrt{T_{T1}}}$$

- Compression ratio (total to total): [-]

$$\beta_{TT} = \frac{p_{T2}}{p_{T1}}$$

- Reduced mass flow rate: [kg/s]

$$M_{cr} = \frac{M_c \cdot p_0 \cdot \sqrt{T_{T1}}}{p_{T1} \cdot \sqrt{T_0}}$$

271   where: T_0 = 293.15 K

272   p_0 = 0.981 bar

273

274   -   Isentropic total-to-total efficiency: [-]

275

$$\eta_{cTT} = \frac{T_{T2s} - T_{T1}}{T_{T2} - T_{T1}}$$

276

277

278   The compressor performance curves are measured from the choking zone to the surge line
279   changing the external circuit characteristic through a motorized throttle valve located downstream
280   of the compressor (Figure 1). The surge condition is identified recording the downstream
281   instantaneous pressure signal to detect the surge frequency through a Fast Fourier Analysis [30].
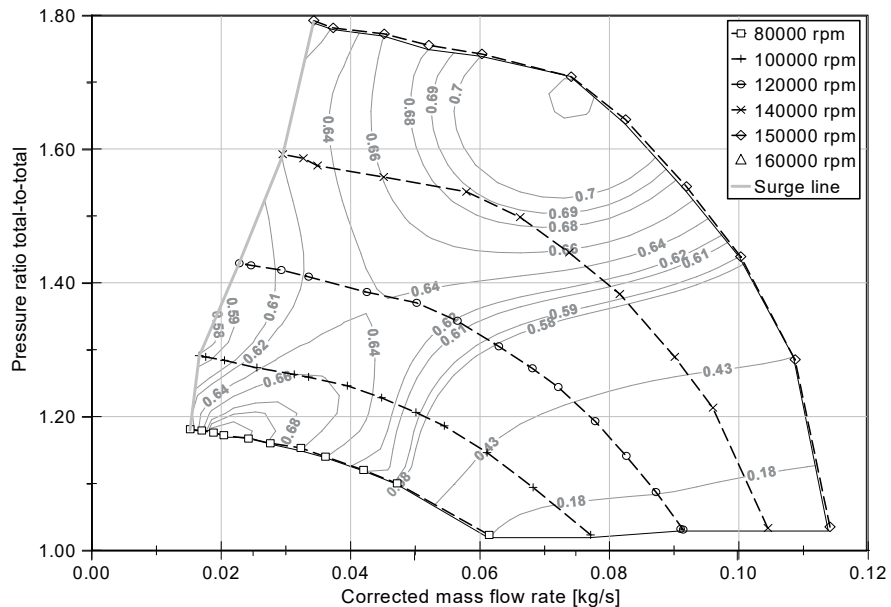
282

283   **Fig. 3: Measured compressor steady flow map.**

284

285   Engine simulation activities described in this paper have been developed referring to the above
286   reported turbines and compressor maps. Simulations are performed referring to ICE "fixed point"
287   and "multiple points" strategies, taking into account different turbocharger configurations (see
288   Table 1), as better explained in the "*ICE modelling and simulation*" section. In particular, to satisfy
289   massflow rates and boost pressure required by the simulated ICE, the similitude scaling approach
290   has been applied to reproduce the appropriate characteristic curve.

291   Both turbines were coupled to the same compressor, scaled in similitude with respect to the tested
292   machine (Figure 3), adopting a mass flow multiplier of 0.75. At the same level of compressor
293   pressure ratio and thermodynamic inlet conditions, the same efficiency value was assumed,
294   neglecting a possible slight increase of boundary layer losses due to the lower compressor size. A
295   third turbine map (called C, in Table 1) was also considered scaling the turbine A map in similitude,

296 adopting a mass flow upscaling of 1.6. Also in this case, the efficiency was maintained unchanged,
297 even if turbine efficiency gradually improves with size.

298

Model name	Compressor	Turbine
Reference TC (fixed point investigation)	massflow scaling 0.75	A
ETC (fixed point investigation)	massflow scaling 0.75	B
Baseline engine (multiple points investigation)	massflow scaling 0.75	A
ETC-ICE (multiple points investigation)	massflow scaling 0.75	C (massflow scaling 1.6 – Turbine A)

299 **Tab. 1: TC Specifications.**

300
301

3. ICE modelling and simulation

303 A twin-cylinder, 0.9 litre, PFI turbocharged SI engine is modelled using AVL Boost® code. The ICE
304 specifications are listed in Table 2.

305

Displacement volume	894 cm^3
Stroke	84.6 mm
Bore	82.0 mm
Connecting Rod lenght	154.0 mm
Compression ratio	8.5

306 **Tab. 2: ICE Specifications.**

307

308 Geometrical and functional ICE characteristics come from a validated and verified Boost model
309 [34]. Valve flows, injector specifications, pipe sizes, element temperatures and friction features
310 result from manufacturer data and Boost library.

311 The model includes an air cleaner, a turbocharger and an air cooler in the intake system. The
312 throttle is replaced by a restriction in the intake plenum inlet pipe. The exhaust system consists of a
313 *"simplified square cell catalyst"* and three different volumes, besides the turbine. Inlet and outlet
314 boundaries are set at normal ambient pressure.

315 Fuel injection system includes two injectors located in the intake ducts just upstream of the intake
316 valves. Gasoline injection is continuous and set to get the required ratio with respect to the air
317 mass-flow measured at Measuring Point 1 (shown in Figure 4).

318 Vibe combustion heat release and Woschni 1978 Heat Transfer models [35] are employed. Perfect
319 mixing model is selected for the scavenging process.

320 The most important modification to the original AVL model is the replacement of the turbocharger
321 *"simplified model"* with the *"full model"*. In the simplified model the turbocharger simulation is
322 performed using the *"waste gate calculation"* mode, which means that the waste-gate mass flow

323 rate is calculated from the target pressure ratio across the compressor, the turbocharger efficiency
324 and the turbine size, while compressor and turbine maps are not needed. The full model gives a
325 more detailed description of turbocharger behaviour and requires the implementation of both
326 compressor and turbine maps.

327 Simulations are performed referring to ICE fixed point and multiple points strategies taking into
328 account different turbocharger configurations, as reported in Tab.1. The ICE fixed point strategy is
329 typical of a range extender configuration, while the multiple points is correlated to a standard
330 vehicle application.

331 Both ICE models are developed in Boost environment: one refers to a classical turbocharger
332 configuration with waste-gate valve while the other considers the use of an ETC consisting of an
333 electric drive connected to the shaft of a fixed-geometry TC without waste-gate valve. This type of
334 ETC is modelled in the Boost code by coupling the turbocharger to an electric machine, which is
335 represented by a specific module (Figure 4) characterized by an efficiency level of 100% since its
336 electrical losses are included in the detailed vehicle model.
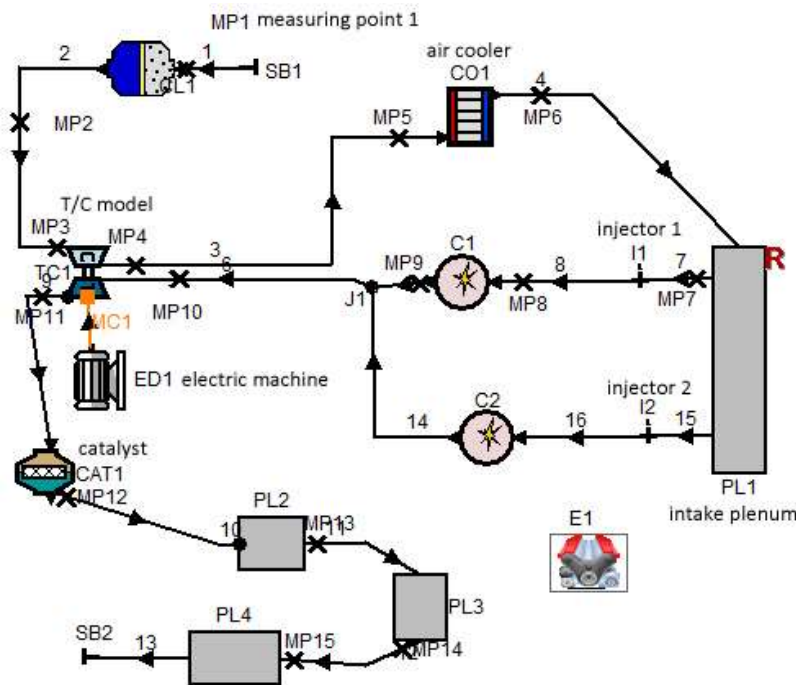
337

338 **Fig. 4: ICE Boost model, Electric Turbo Compound version.**

339

340 *3.1 Fixed point simulation results*

341 Preliminary simulations are conducted at a fixed ICE operating condition (as in the case of range-
342 extended vehicles) as reported in Table 3. Starting from 1500 rpm, 1.53 bar absolute boost
343 pressure and 14.5 A/F ratio, reference TC and ETC are compared. In the case of "reference TC",
344 turbine A is properly sized to supply only the power necessary for the compressor. For "ETC"
345 simulation a turbine able to furnish more power is selected (turbine B in Tab.1), therefore the extra
346 power provided is collected by the electric machine. However, in the absence of ETC, a waste gate
347 strategy must be applied with turbine B (case "reference sim" in Table 3).

348 Other points at higher ICE rpm are simulated both for "reference TC" and "ETC" with turbine B, as
349 shown in Table 3. At 1500 rpm the best overall efficiency is obtained with the ETC generating 0.28
350 kW of electrical power. However, with respect to the reference TC, ICE efficiency is affected by
351 increased exhaust backpressure, thus the reduction of total specific fuel consumption turns out to
352 be unsubstantial (only 1%, without considering electrical losses).

353 At 2000 rpm and 1.65 bar, corresponding to the best ICE efficiency with reference TC, ETC
354 provides a slight improvement, less than 2%, in terms of total BSFC. Increasing the rotational
355 speed, 3000 and 4000 rpm, ETC effect becomes negative due to the exhaust backpressure raised
356 to unacceptable level, suggesting the adoption of a turbine with increased swallowing capacity for
357 this application.

358

	WG bypass	Rot. speed	Boost press.	Air massflow	ICE power	ETC power	ICE BSFC	Tot BSFC	Exhaust backpressure	Turbine
	%	rpm	bar	kg/s	kW	kW	g/kWh	g/kWh	bar	
Reference TC	0	1500	1.53	0.0170	17.00	-	248.37	248.37	1.21	(A)
Reference sim	15	1500	1.53	0.0170	16.90	-	248.99	248.99	1.26	(B)
ETC	0	1500	1.53	0.0170	16.90	0.28	250.59	246.51	1.31	(B)
Reference TC	22	2000	1.65	0.0247	24.78	-	248.07	248.07	1.41	(B)
ETC	0	2000	1.65	0.0246	24.30	0.80	251.62	243.60	1.53	(B)
Reference TC	40	3000	1.64	0.0382	37.41	-	253.73	253.73	1.53	(B)
ETC	0	3000	1.65	0.0385	35.10	2.25	275.00	258.43	1.94	(B)
Reference TC	47	4000	1.64	0.0507	47.44	-	266.07	266.07	1.66	(B)
ETC	0	4000	1.65	0.0510	41.98	3.51	301.00	277.77	2.32	(B)

359
360 **Tab. 3: Comparison for engines operating at fixed point**
361
362

363 ### 3.2 Multiple points simulation results

364 ICE behaviour in standard vehicle application is simulated referring to a classical turbocharger
365 configuration with waste-gate valve and then compared to the same engine equipped with an ETC.

366 Baseline cases for 24 different operating conditions are considered and reported in Table 4.
367 Corresponding Brake Specific Fuel Consumption (BSFC) results are shown in map of Figure 5.

368 Simulations at the same operating conditions of the ICE fitted with ETC are reported in Table 5.
369 The simulated steady points are similar, with the exception of full load 800 and 1500 rpm: at low
370 speeds and full load ETC system is used to achieve higher power levels.

371

372

load	ICE speed (rpm) @ intake manifold pressure (bar)						Turbine
100%	800 @ 1.31	1500 @ 1.53	2000 @ 1.65	2500 @ 1.65	3000 @ 1.64	4000 @ 1.63	(A)
ca. 80%	800 @ 1.17	1500 @ 1.30	2000 @ 1.30	2500 @ 1.29	3000 @ 1.30	4000 @ 1.29	(A)
ca. 60%	800 @ 1.00	1500 @ 1.00	2000 @ 1.00	2500 @ 1.00	3000 @ 1.00	4000 @ 1.00	(A)
ca. 25% (throttled)	800 @ 0.61	1500 @ 0.60	2000 @ 0.60	2500 @ 0.61	3000 @ 0.60	4000 @ 0.59	(A)

373
374 **Tab. 4: baseline simulated cases.**
375

376
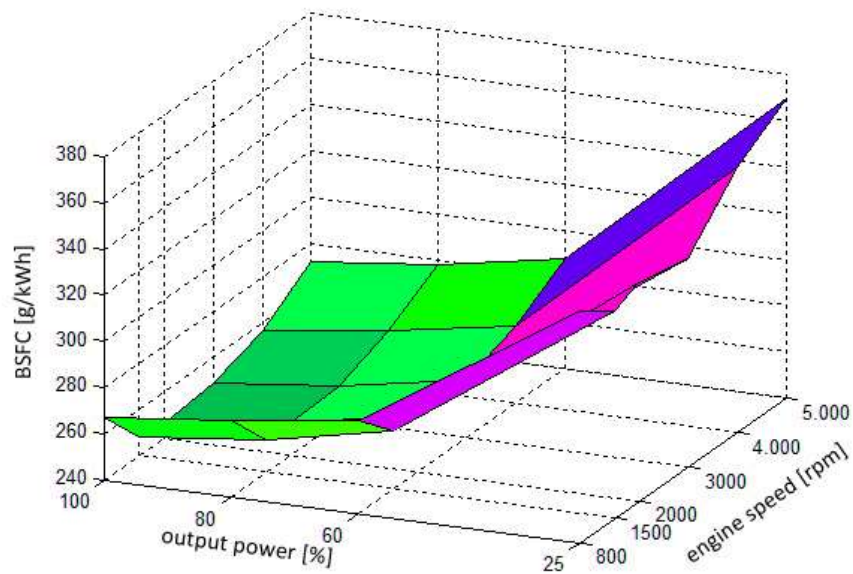
377 **Fig. 5: Baseline BSFC Map**

378

379 The turbocharger turbine (C) is characterized by a larger size (+60% swallowing capacity scaling,
380 in similitude) than in the baseline case in order to limit the backpressure at ICE high speeds and
381 loads, despite the absence of waste-gate valve. Therefore, at low ICE rotational speed levels the
382 fixed geometry turbine cannot give enough energy to drive the compressor, energy which is
383 supplied by the electric device.

384

load	ICE speed (rpm) @ intake manifold pressure (bar)						Turbine
100%	800 @ 1.41	1500 @ 1.65	2000 @ 1.65	2500 @ 1.66	3000 @ 1.66	4000 @ 1.65	(C)
ca. 80%	800 @ 1.19	1500 @ 1.30	2000 @ 1.30	2500 @ 1.30	3000 @ 1.31	4000 @ 1.30	(C)
ca. 60%	800 @ 1.00	1500 @ 1.00	2000 @ 1.00	2500 @ 1.00	3000 @ 1.00	4000 @ 1.00	(C)
ca. 25% (throttled)	800 @ 0.61	1500 @ 0.61	2000 @ 0.59	2500 @ 0.61	3000 @ 0.61	4000 @ 0.60	(C)

385
386 **Tab. 5: ETC-ICE simulated cases.**

To compare the baseline case with the ETC-fitted ICE, total power, evaluated as the sum of the engine power and the electrical power with 100% electric drive efficiency, is plotted in Figure 6 versus rotational speed. As it can be observed, a slight improvement of total power occurs at mid-low ICE rotational speed levels and increases with ICE speed, due to the larger exhaust gas mass-flow rate providing, on the TC group, an extra power recovered by the electrical machine.
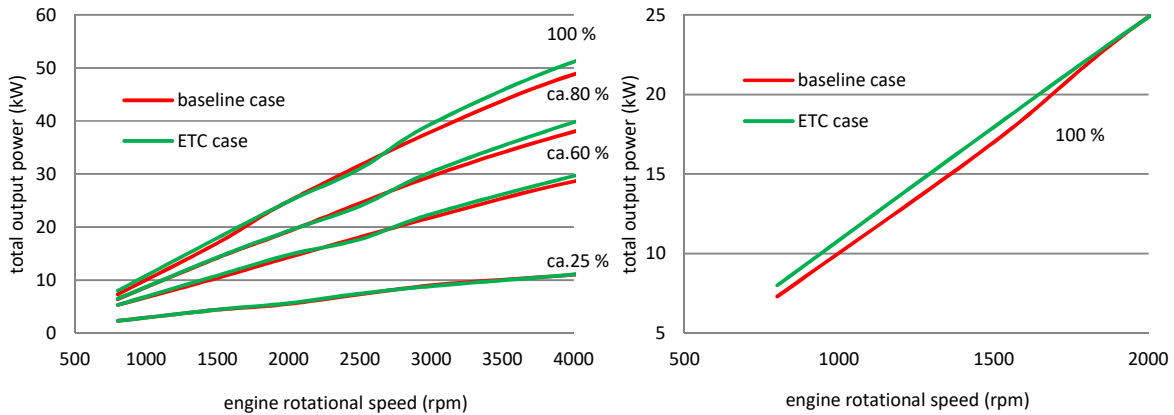

Fig. 6: Total output power - comparison between baseline and ETC-ICE, at full power, ca.80% ca.60%, ca.25%. Focus on full load, low rpm.

At ICE full load condition (Figure 7), the electric drive acts as motor below 2500 rpm assisting the turbocharger to achieve the required boost pressure. Over 2500 rpm, the electric drive works as generator 'braking' the turbocharger and collecting the energy surplus provided by the turbine. In the cases of ca. 80% and ca. 60% of full load, the electric drive is always keeping energy from the turbocharger. Below ca.60% of full load (Figure 7) the ECU (Engine Control Unit) switches from boost pressure control to classical intake throttling. In these conditions the amount of exhaust gas energy rapidly falls down and the ETC recovers only small amounts of energy, with no influence on total specific fuel consumption (which takes total power into account).
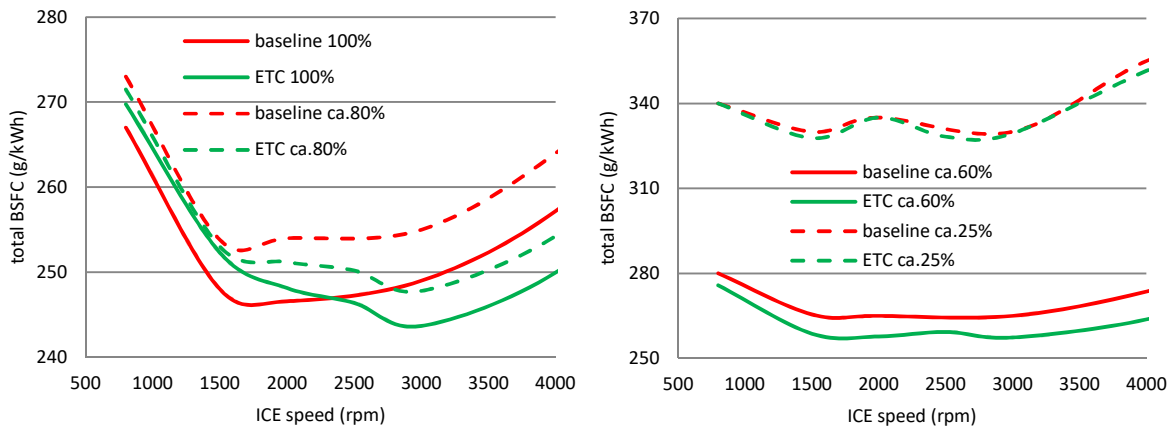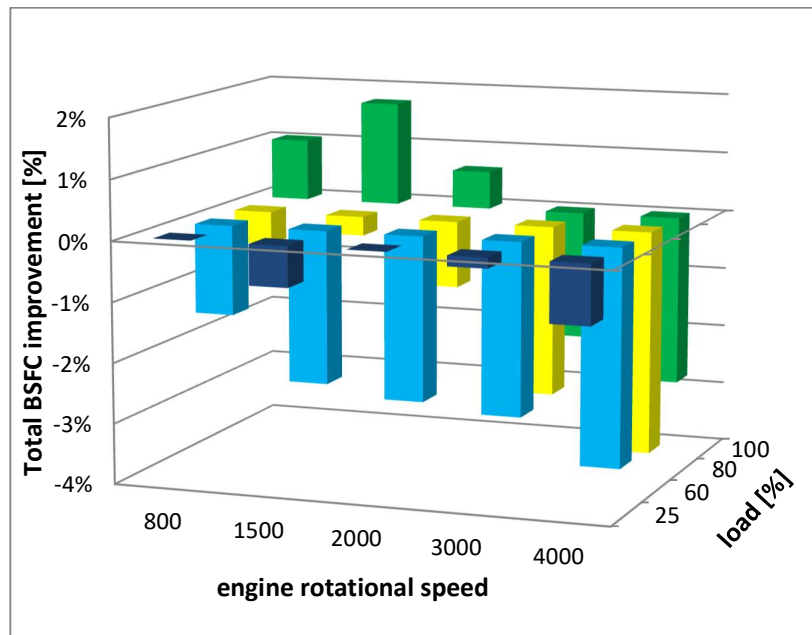

Fig. 7: Total Brake Specific Fuel Consumption - comparison between baseline and ETC-ICE at various loads.

408   In Figure 8 the baseline BSFC is compared with the total BSFC of the ETC-fitted ICE at same
409   operating conditions. In forced induction conditions (above ca.60% of full load) moderate
410   reductions of fuel consumption occur at every ICE rotational speed level. Only at ICE rotational
411   speeds below 2000 rpm at full load, a slight increase arises due to electric power spent to achieve
412   the boost pressure target. On the other hand the boost pressure reached is higher than in the
413   baseline case, with obvious advantage in terms of power output. In naturally aspirated conditions
414   (below ca.60% of full load), only negligible BSFC improvements occur.

415

417   **Fig. 8: Percentage variation of total Brake Specific Fuel Consumption - comparison between baseline**
418   **and ETC-ICE at various loads.**
419

420   ## 5. Powertrain architecture

421   The activity, initially focused on the ICE and the TC group, moves to the whole powertrain
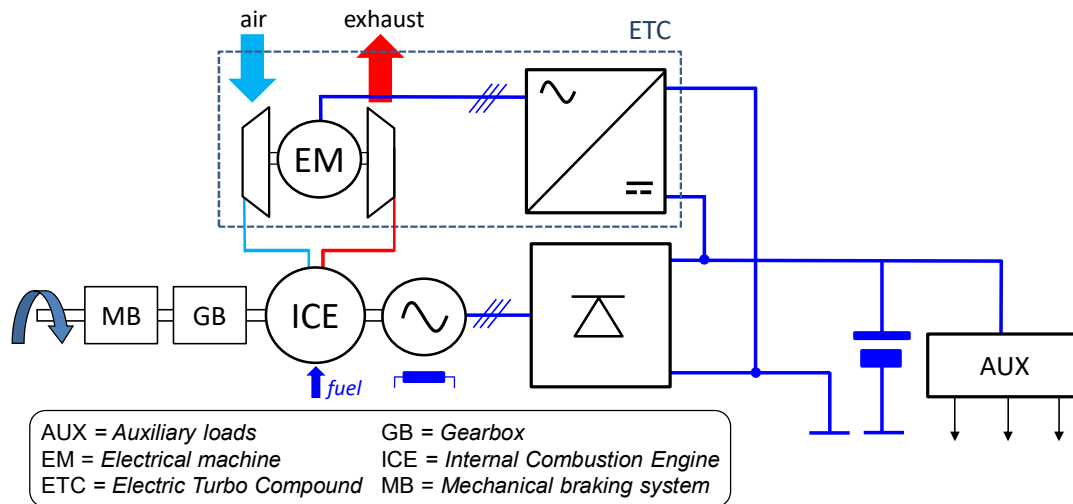422   modelling, to verify the effectiveness of the proposed solution.

423   As in the solution currently in use in the F1 Championship, the ETC system can be used in an
424   hybrid powertrain [36,37]. However, as first approach, the powertrain architecture has been
425   maintained, as far as possible, the same of a conventional vehicle equipped with a standard TC
426   group. The conventional electrical system is kept unchanged, apart from the introduction of the
427   ETC system. A sketch is shown in Figure 9.

428   The electrical machine of the ETC system to convert the excess of exhaust energy into electricity is
429   directly coupled to the shaft of the standard TC group. On the other hand, The alternator is coupled
430   to the ICE and interfaced with the DC network through a rectifier bridge, to feed the auxiliary loads.
431   The conventional alternator, the rectifier bridge, the SLI battery and the electrical auxiliary loads
432   are kept unchanged.

433   It must however be mentioned that the rectifier bridge could be replaced with a bidirectional
434   converter, to allow the electricity produced by the ETC to be converted back into mechanical

energy at the alternator pulley. This option could be considered when the electrical energy generated by the ETC is so large that, in the case of low energy consumption by the auxiliary loads, the standard SLI battery is inadequate to store it all. On the contrary, for small amounts of generated energy, the cheaper diode rectifier bridge is sufficient, and the SLI energy is totally stored inside the battery. We adopt the diode bridge solution, because simulations show that in our case the available ETC electrical energy can always be effectively stored in the battery.

AUX = *Auxiliary loads*   GB = *Gearbox*
EM = *Electrical machine*   ICE = *Internal Combustion Engine*
ETC = *Electric Turbo Compound* MB = *Mechanical braking system*

Fig. 9: Powertrain Architecture

6.   Powertrain modelling and simulation

The modelling of the selected architecture is performed by means of a suitable powertrain simulation model, built for carrying out fuel consumption analysis. The model is of the forward type, since the vehicle trip is determined as a consequence of driver commands.

The model is conceived using 3DS's Dymola [38], based on Modelica language [39]. In addition to the conventional powertrain, it includes the electric turbo compound (ETC). The results obtained with the model for the vehicle equipped with the ETC system are compared with those relative to the conventional version, mainly to evaluate energy flows and fuel consumption.

6.1 The simulation model

The different subsystems are modelled weighting accuracy and complexity for the considered purpose. In particular, since the fastest transients in the powertrain model show time constants in the order of 100 ms, much faster phenomena such as combustion dynamics or valve switching inside electronic converters are considered to be algebraic.

Hereinafter, a brief description of the main model subsystems is presented.

The internal combustion engine (ICE) model evaluates the fuel consumption and torque as an algebraic function of engine speed and throttle position; the generated torque is applied to a submodel simulating the mechanical inertia. The model fuel flow control includes over-run cut off and idle speed control. The fuel consumption and torque values are obtained from the ICE modelling activity previously described, both in the conventional configuration equipped with the standard TC group, and in the other one, equipped with the ETC system. The values differ mainly due to the different ambient conditions at the inlet and exhaust engine ports. In fact, as detailed in the previous paragraph, the waste gate valve is considered only in the standard TC group, while it is removed in the ETC system. The effects, being the fluidic ports not included in the considered model, are indeed directly considered in fuel consumption and torque functions.

The ETC model contains a permanent-magnet synchronous machine (EM) and an electronic converter. Still because the fluidic model of the TC group is not represented in the model, the values of torque and rotary speed given by the ICE modelling activity, which depend on throttle and ICE rotational speed, have been directly imposed to the pulley of the electrical machine. A general representation of the two models is shown in Figure 10. The main electrical machine parameters are shown in Table 6. Some analysis on design and manufacturing aspects is presented in [40].
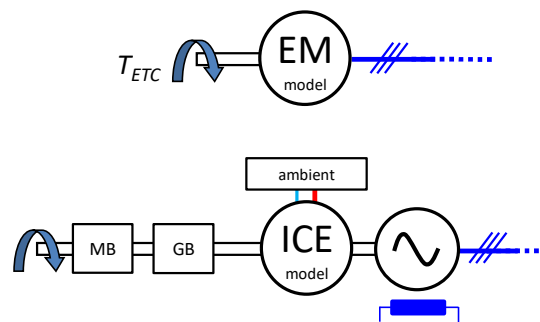
Fig. 10: ETC electrical machine and ICE models

Nominal power (kW)	2
Nominal torque (Nm)	0.5
Nominal speed (rpm)	40 000
Maximum speed (rpm)	160 000
Nominal RMS line voltage (V)	7.8
Nominal current (A)	148
Efficiency @ 80000 rpm (%)	75

Tab. 6: Model parameters for the ETC electrical machine

As regards the three-phase alternator, the model of a conventional machine is used. Maximum DC current is 140 A, maximum speed is 15000 rpm. Alternator and diode bridge losses are taken into account using interpolation formulas; the resulting efficiency is 75% at 7500 rpm.

486 The vehicle is modelled through a mechanical equation describing its longitudinal behaviour.
487 Resistance force is modelled as a second-order polynomial, to take into account rolling resistance
488 ad aerodynamic drag. Furthermore, the transmission model is composed by an automatic gearbox
489 including a torque converter with a lock-up clutch. The gearbox is modelled as a series of fixed
490 gear ratios, following the approach shown in [41], that are shifted according to a specific control
491 logic. In particular, the control logic determines the shift point based on throttle position and vehicle
492 speed, according to a predefined shift map. Typical available values for the vehicle under study are
493 employed [42]. To ease the comparison between the standard and the new powertrain
494 configuration, standard gear ratios and control shift strategy are kept unchanged.

495

6.2 Energy management strategy

497 The main purpose of the energy management strategy is, besides interpreting the driver requests
498 and feeding the electrical auxiliary loads, to manage the electrical energy, in order to allow the
499 battery to receive the excess power generated by the ETC with respect to the amount needed by
500 the auxiliary loads. Therefore, the power management module (PMM) has the fundamental roles
501 to:

502 • interpret the driver brake/accelerator commands and convert them in terms of torque request;

503 • keep the battery voltage at a level close to that of conventional cars, since the standard
504 electrical system is unchanged;

505 • guarantee a battery SOC that makes the battery capable to accept all the available
506 regenerative braking energy. In fact, nevertheless the problem mainly involves hybrid and
507 electric vehicles, some modest energy recovery can be ensured also in conventional ones. A
508 comprehensive description of the problem is shown also in [43,44].

509 A schematic implementation of the described roles is shown in Figure 11. The driver model is a
510 Proportional-Integral controller with some additional elements to better model the actual driver
511 behaviour. In fact, the PI determines the torque request based on the error between actual and
512 wished speed, and torque request is split into two signals corresponding to the accelerator and
513 brake pedal positions. Therefore, the driver only controls one pedal at a time and does not jump
514 rapidly from the throttle to the brake pedal. The driver model parameters, that already represent an
515 average driver behaviour, are maintained at their defaults.

516 The accelerator request goes directly to an electronic control unit (ECU), which regulates the fuel
517 and the air flows. On the other hand, the brake request signal needs to be further split into
518 regenerative and dissipative braking components. When the torque request is slightly negative, i.e.
519 the brake pedal is slightly pushed, this torque is only obtained by means of an increase of the
520 alternator load that produces electrical braking and the mechanical brakes are not activated: this is
521 obtained by means of the dead-band non-linear block in the signal path that generates T_{MB}.

522 Sole electrical braking is kept as far as the maximum torque of the alternator is achieved (see the
523 saturation block shown in Figure 11), or the battery is fully charged. When stronger braking is
524 needed, mechanical braking must be added. This occurs when the brake request signal is higher
525 than the dead-band zone of the block feeding T_{MB}.

526 To accomplish the other PMM role, i.e. to keep the battery voltage close to the usual level of
527 conventional cars, and to ensure a SOC that allows the battery to accept the braking energy, the

528 DC voltage reference is maintained slightly below 14 V. This is implemented through a PI controller
529 (the PI block shown in Figure 11), having the battery SOC reference (SOC^*) around 0.9.

530 The torque reference T_{ED}, composed by the output of the PI controller and the additional term due
531 the regenerative braking, acts directly on the electronic control unit (ECU) of the electrical machine.
532 The ECU, taking into account the alternator rotary speed (Ω), determines the requested excitation
533 current I_{ecc}.
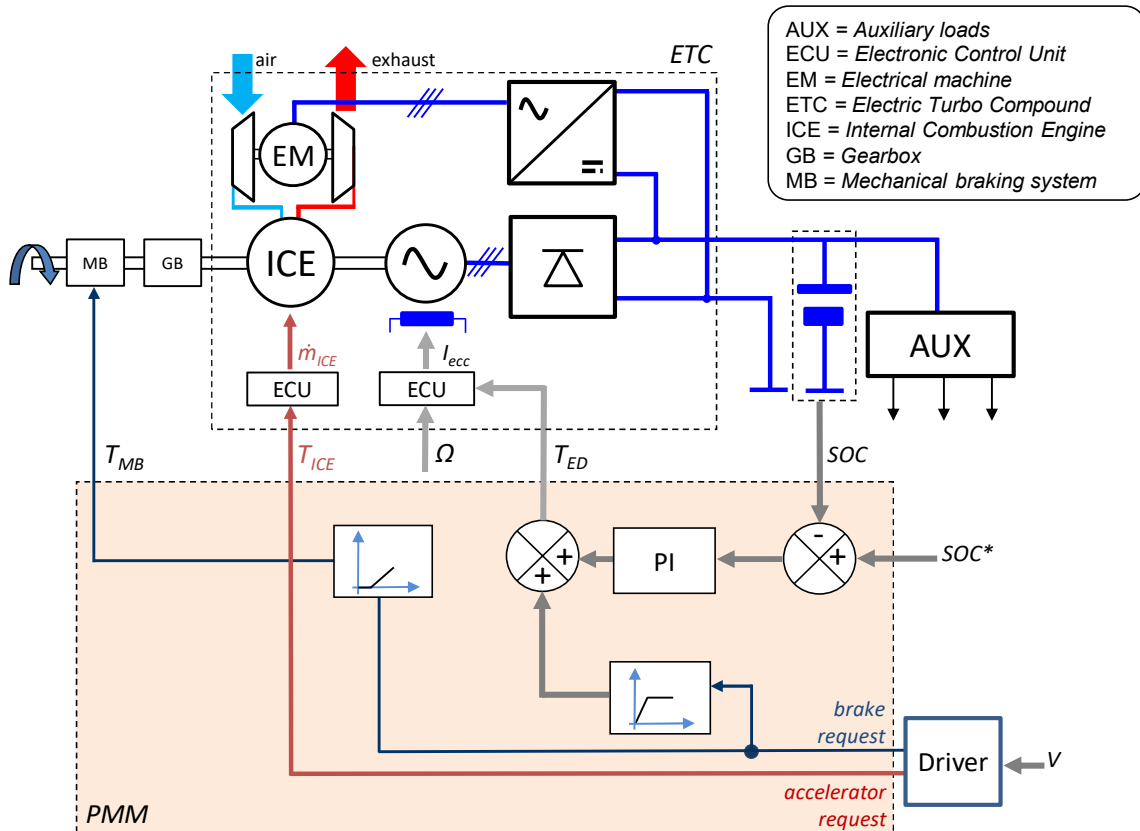
534
535 **Fig. 11: Energy management strategy**

6.3 Powertrain simulation results

537 The simulations are performed considering three driving cycles and two different vehicle
538 configurations, to properly analyse the ETC system under different working conditions. The three
539 driving cycles, all from CADC (Common Artemis Driving Cycle), are described in Table 7 and
540 shown in Figure 12. These cycles, differently from other standard cycles as NEDC (New European
541 Driving Cycle) considered in [40], are able to represent the vehicle usage in urban, extra-urban
542 roads and motorways in a realistic way. Further details about CADC are shown in [45].

	Urban	Rural Road	Motorway
Duration (s)	920	1081	1067
Distance (km)	4.5	17.3	29.6
Average speed (km/h)	17.5	57.5	99.7
Maximum speed (km/h)	58	112	150
Speed distribution (%)			
Idle	29	3	2
Low speed ($0<v<50$)	69	31	15
Medium speed ($50<v<90$)	2	59	13
High speed ($v>90$)	0	7	70

Tab. 7: Characteristics of CADCs (Common Artemis Driving Cycles)
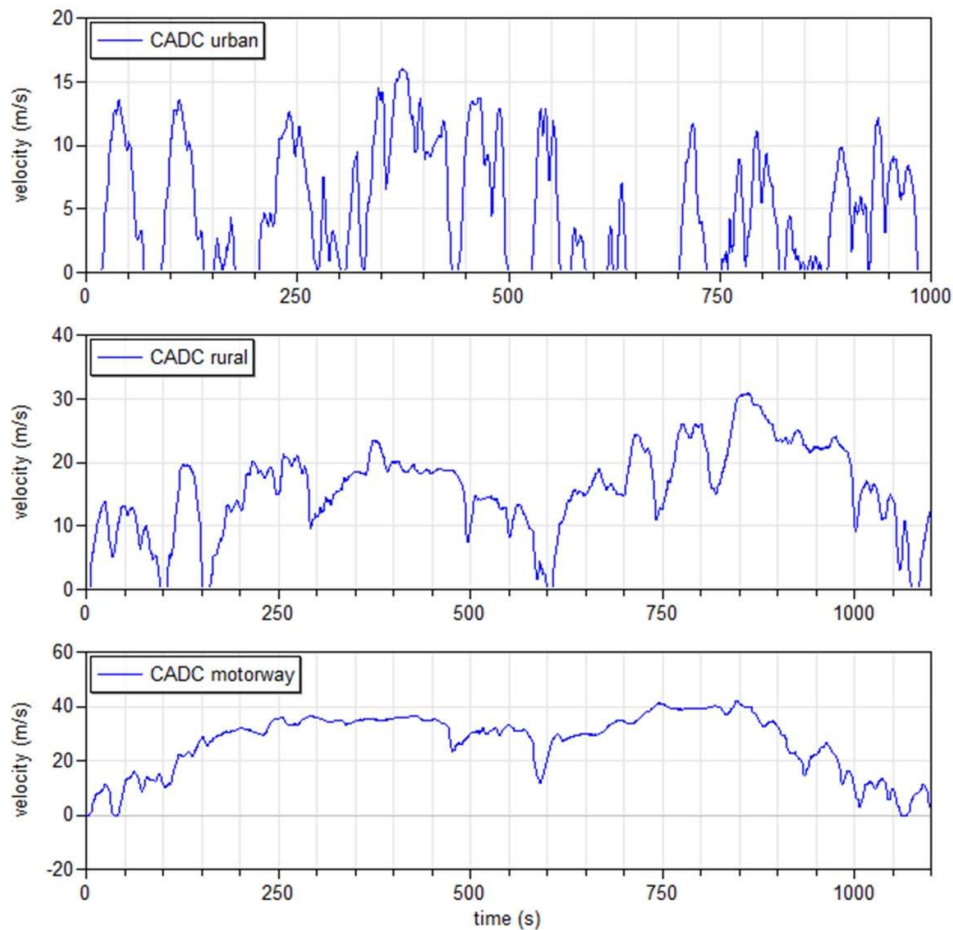
**Fig. 12: CADC (Common Artemis Driving Cycle) urban, rural, motorway**

Two different vehicle configurations are considered: the first one, representative of a small medium car, the second one typical of a top medium car. The details are shown in Table 8. Regarding the electrical auxiliary loads, from analysis of literature [46] an average value of 350 W is considered.

	Mass (kg)	1200
Small medium	Frontal area (m²)	1.8
	Cx	0.31
	Mass (kg)	1700
Top medium	Frontal area (m²)	2.0
	Cx	0.28

551
552   **Tab 8: Vehicle model parameters**
553

554   Figure 13 shows mechanical power and rotary speed of the ETC electrical machine, during a
555   portion of the CADC rural. It shows that during the ICE acceleration transients almost at full load,
556   the ETC works as generator producing electrical energy (i.e. the mechanical power assumes
557   negative values), while during braking or at idle speed it works as motor (i.e. the mechanical power
558   is positive), keeping the turbocharger unit at the desired speed by compensating the energy
559   losses.
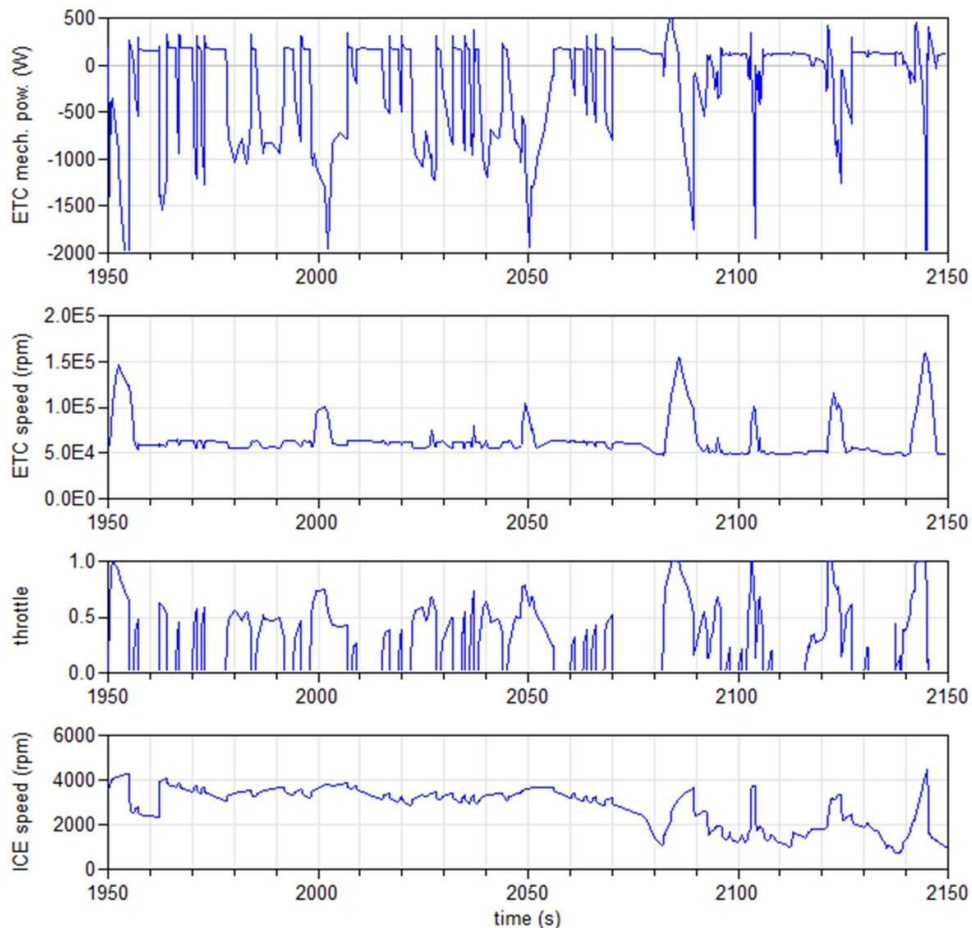
560
561   **Fig. 13: ETC mechanical power and rotary speed, ICE throttle, ICE rotary speed,**
562   **top medium car, portion of CADC rural**

563   Figure 14 shows the generated DC electrical power. During acceleration and drive at constant
564   speed, the generator works to fulfil the auxiliary load requests. During braking, because of the

additional term in the control logic previously described, the generated electric power rises up. However, according to the control logic adopted, the battery SOC (state of charge) remains under control.
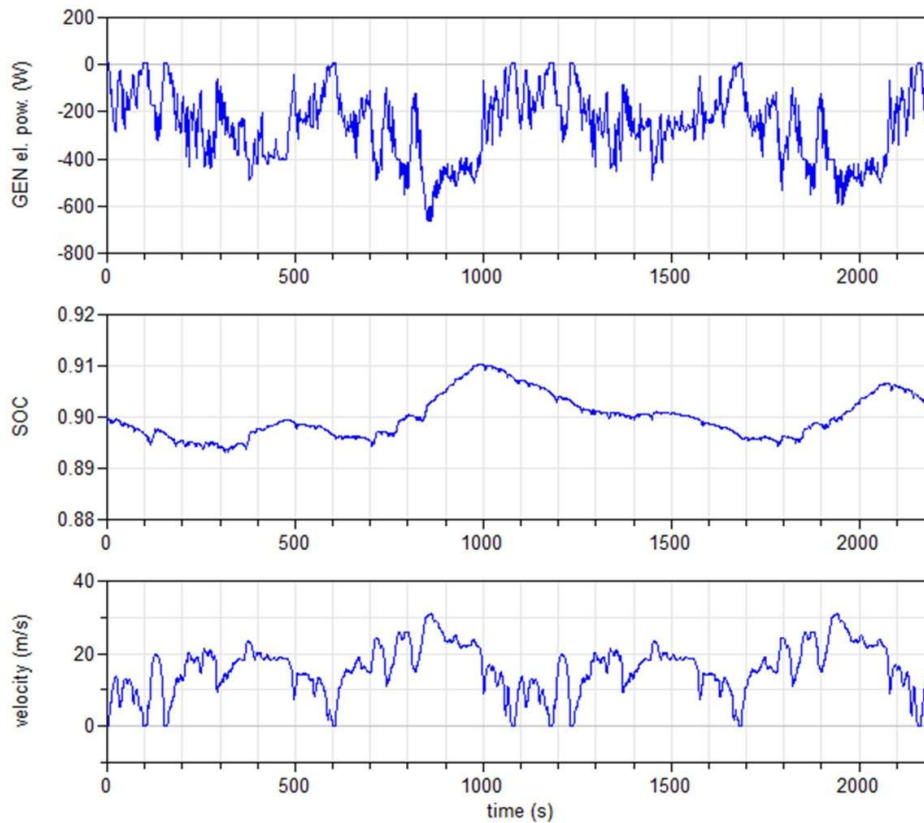
Fig. 14: Generator DC electrical power, battery SOC, top medium car, CADC rural (two cycles represented)

Finally, the fuel consumption results are related to the examined two vehicle configurations, performing the three considered CADC cycles (i.e. urban, rural and motorway). Simulation have been firstly performed for the standard TC group configuration, then considering the ETC system. Results are shown in Table 9. Variation refers to the percentage difference, in terms of coverage distance per litre, of the vehicle equipped with the ETC system in comparison with the baseline TC configuration.

Vehicle	Cycle	Baseline TC (km/L)	ETC system (km/L)	Variation (%)
Small medium	CADC urban	7.7	7.5	-1.9
	CADC rural	14.6	14.5	-0.5
	CADC motorway	18.1	18.4	+1.7
Top medium	CADC urban	6.9	6.8	-0.9
	CADC rural	13.4	13.6	+1.5
	CADC motorway	17.0	17.5	+2.7

Tab. 9: Fuel consumption results

The table shows that, the ETC does not improve fuel economy of the smaller vehicle, especially when employed in urban cycles. As a matter of fact, even though the ETC sometimes delivers small amounts of electrical energy, most of the time it requires electrical power to maintain the TC group at the desired boost pressure. In this case, fuel consumptions may even rise up, in comparison with the baseline TC solution.

The ETC is much more advantageous in the case of the larger vehicle, particularly when extra-urban roads or motorways are considered. In fact, under these conditions, engine works mainly in the high loads and rpm region and consequently the ETC delivers significantly larger electrical power that causes an improvement of fuel consumption of around 2.7%.

It must however be noticed that the fuel savings shown in Table 9 are significantly smaller than the value of 4% obtained in the steady state analysis. This is a consequence not only of the fact that during road cycle simulations the operating points of ICE, turbine and compressor vary continuously (and often they are low-efficiency points), but also of the fact that in the steady state analysis the electrical components (alternator, converter, battery) are considered lossless, while in the driving-cycle simulations their losses are taken into account.

7. Summary/Conclusions

The paper relates to a numerical research carried out in cooperation between the Universities of Pisa and Genoa and focused on the evaluation of the benefits resulting from the application of an Electric Turbo Compound (ETC) to a small twin-cylinder SI engine intended for cars with conventional architecture (not hybrid).

Starting from the experimental maps of two turbines and one compressor, the complete model of a turbocharged engine is created using the AVL BOOST one-dimension code. Simulations are performed referring to ICE fixed point and multiple points strategies taking into account different turbocharger configurations. The numerical activity then moves to the whole vehicle/powertrain modelling, considering three driving cycles and two different vehicle configurations, adopting the 3DS's Dymola code based on Modelica language.

When the engine is run at a fixed point (characteristic of a range extender), an electric drive applied to a conventionally optimized TC group leads to unsubstantial reduction of total specific fuel consumption, since ICE efficiency is affected by increased exhaust backpressure.

As regards the engine operating at various speeds and loads (i.e. in standard vehicle application) and adopting proper turbine sizing, application of ETC is able to produce a moderate efficiency improvements, up to 4% of total brake specific fuel consumption, depending on engine speed and load. However, ETC leads to benefits as regards boost region extension to the lowest ICE rotational speeds and possible turbo lag reduction.

Concerning the whole vehicle/powertrain simulation, first results confirm that ETC leads to small changes in fuel saving (up to 2.7%) in the case of top medium-size cars. Moreover, results show that the ETC does not improve fuel economy of the smaller vehicle, especially when employed in urban cycles when the engine is run in the medium-low load and speed conditions. The ETC is much more advantageous in the case of the larger vehicle, particularly when motorway cycles are considered, since the engine works in the region of high loads and speeds

Future study will be conducted on other solutions involving ETC, such as its application to compression-ignited ICEs, two-stage turbocharging, turbine and compressor without mechanical link, both with individual electric drive.

References

[1] Mohd Noor A., Che Puteh R., Rajoo S., "*Waste Heat Recovery Technologies In Turbocharged Automotive Engine – A Review*", Journal of Modern Science and Technology, Vol.2 No.1, 108-119, March 2014.

[2] Saidur R., Rezaei M., Muzammil W.K., Hassan M.H., Paria S., Hasanuzzaman M., "*Technologies to recover exhaust heat from internal combustion engines*", Renewable and Sustainable Energy Reviews 16, 5649-5659, 2012.

[3] Hountalas D.T., Katsanos C.O., Kouremenos D.A., Rogdakis E.D., "Study of available exhaust gas heat recovery technologies for HD diesel engine applications", Int Journal of Alternative Propulsion 1, 228–49, 2007.

[4] Weerasinghe W.M.S.R., Stobart R.K., Hounsham S.M., "*Thermal efficiency improvement in high output diesel engines: a comparison of a Rankine cycle with turbo-compounding*", Applied Thermal Engineering 30, 2253-2256, 2010.

[5] Park T., Teng H., Hunter G.L., Van Der Velde B., Klaver J., "*A Rankine cycle system for recovering waste heat from HD Diesel Engines – Experimental results*", SAE Paper no. 2011-01-1337; 2011.

[6] Wang T., Zhang Y., Peng Z., Shu G., "*A review of researches on thermal exhaust heat recovery with Rankine cycle*", Renewable and Sustainable Energy Reviews 15, 2862-2871, 2011.

[7] Sprouse C., Depcik C., "*Review of organic Rankine cycles for internal combustion engine exhaust waste heat recovery*", Applied Thermal Engineering 51, 711-722, 2013.

[8] Hossain S.N., Bari S., "*Waste heat recovery from the exhaust of a diesel generator using Rankine Cycle*", Energy Conversion and Management 75, 141-151, 2013.

[9] Tahani M., Javan M., Biglari M., "A comprehensive study on waste heat recovery from internal combustion engines using organic rankine cycle", Thermal Science, 2013, Vol. 17, No. 2, pp. 611-624.

[10] Tchanche B. F., Lambrinos Gr., Frangoudakis A., Papadakis G.,"*Low-grade heat conversion into power using organic Rankine cycles – A review of various applications*", Renewable and Sustainable Energy Reviews 15, 2011, 3963-3979.

[11] Bass J.C., Kushch A.S., Elsner N.B., "*Thermoelectric generator (TEG) on heavy diesel trucks*", Proceedings ICT2001. 20° International Conference on Thermoelectrics, Beijing, 2001.

[12] Rowe M. D., "*Thermoelectric waste heat recovery as a renewable energy source: Review*", Int. J. Innov. Energy Syst. Power 1, 2006,13-23.

[13] Fairbanks J., "*Thermoelectric applications in vehicles status 2008*", In: 6th European Conference of Thermoelectrics, Paris, France 2008.

[14] Gou X., Yang S., Xiao H., Ou Q., "*A dynamic model for thermoelectric generator applied in waste heat recovery*", Energy 52, 2013, 201-209.

[15] Shuhai Y., Qing D., Hai D., Gequn S., Kui J., "*Effect of vehicle driving conditions on the performance of thermoelectric generator*" Energy Conversion and Management 96, 2015, 363-376.

[16] Zhao R., Zhuge W., Zhang Y., Yin Y., Chen Z., Li Z., "*Parametric study of power turbine for diesel engine waste heat recovery*", Applied Thermal Engineering 67, 2014, 308-319.

668 [17] Callahan T.J., Branyon D.P., Forster A.C., Ross M.G., Simpson D.J., "*Effectiveness of*
669 *Mechanical Turbo Compounding in a Modern Heavy-Duty Diesel Engine*", International
670 Journal of Automotive Engineering 3, 69-73, 2012.

671 [18] Boretti A., "*Conversion of a heavy duty truck diesel engine with an innovative power turbine*
672 *connected to the crankshaft through a continuously variable transmission to operate*
673 *compression ignition dual fuel diesel-LPG*", Fuel Processing Technology 113, 97-108, 2013.

674 [19] Zhao R., Zhuge W., Zhang Y., Yang M., Botas R. M., Yin Y., "*Study of two-stage turbine*
675 *characteristic and its influence on turbo-compound engine performance*", Energy Conversion
676 and Management 95, 2015, 414-423.

677 [20] Aman M.I., Romagnoli A., Ricardo F., M.-B., "*Characterisation of a low pressure turbine for*
678 *turbocompounding applications in a heavily downsized mild-hybrid gasoline engine*", Energy
679 64, 2014, 3-16.

680 [21] Cipollone R., Di Battista D., Gualtieri A., "*Turbo compound systems to recover energy in ICE*",
681 International Journal of Engineering and Innovative Technology (IJEIT) Volume 3, Issue 6,
682 December 2013.

683 [22] Briggs I., McCullough G., Spence S., Douglas R. "*Whole-vehicle modelling of exhaust energy*
684 *recovery on a diesel-electric hybrid bus*", Energy 65, 2014, 172-181.

685 [23] Katsanos C.O., Hountalas D.T., Zannis T.C., "*Simulation of a heavy-duty diesel engine with*
686 *electrical turbocompounding system using operating charts for turbocharger components and*
687 *power turbine*", Energy Conversion and Management 76, 2013, 712-724.

688 [24] Newman P., Luard N., Jarvis S., Richardson S., Smith T., Jackson R., Rochette C., Lee D.,
689 Criddle M., "*Electrical supercharging for future diesel powertrain applications*", 11th
690 International Conference on Turbochargers and Turbocharging, The British Museum, London,
691 2014, Pages 207–216.

692 [25] Terdich N., Ricardo M.B., "*Experimental Efficiency Characterization of an Electrically Assisted*
693 *Turbocharger*", SAE Technical Paper 2013-24-0122, 2013, doi:10.4271/2013-24-0122.

694 [26] Hopmann U., Algrain M., "*Diesel Engine Electric Turbo Compound Technology*", SAE
695 Technical Paper 2003-01-2294, 2003, doi:10.4271/2003-01-2294.

696 [27] Millo F., Mallamo F., Pautasso E., Ganio Mego G., "*The Potential of Electric Exhaust Gas*
697 *Turbocharging for HD Diesel Engines*", SAE Technical Paper 2006-01-0437, 2006.

698 [28] Zhuge W., Huang L., Wei W., Zhang Y. et al., "*Optimization of an Electric Turbo Compounding*
699 *System for Gasoline Engine Exhaust Energy Recovery*", SAE Technical Paper 2011-01-0377,
700 2011

701 [29] Wei W., Weilin Z., Yangjun Z., Yongsheng H., "*Comparative Study on Electric Turbo-*
702 *Compounding Systems for Gasoline Engine Exhaust Energy Recovery*", ASME Turbo Expo:
703 Power for Land, Sea, and Air, Paper No. GT2010-23204, pp. 531-539, 2010.

704 [30] Marelli S., Carraro C., Marmorato G., Zamboni G., Capobianco M., "*Experimental Analysis on*
705 *Steady Flow Performance under Unstable Operating Conditions and on Surge Limit of a*
706 *Turbocharger Compressor*", Experimental Thermal and Fluid Science, Volume 53, pages 154-
707 160, doi: 10.1016/j.expthermflusci.2013.11.025, February 2014.

708 [31] Capobianco M., Marelli S., "Waste-gate turbocharging control in automotive SI engines: effect
709 on steady and unsteady turbine performance", SAE Technical paper, Proceedings of the 14th
710 Asia Pacific Automotive Engineering Conference, ISBN: 9780768019544, doi: 10.4271/2007-
711 01-3543, 2007.

712 [32] Marelli S., Capobianco M., "*Experimental Investigation under Unsteady Flow Conditions on*
713 *Turbocharger Compressors for Automotive Gasoline Engines*", Proceedings of the 10th
714 International Conference on Turbochargers and Turbocharging, p. 219-229, ISBN:
715 9780857092090, 2012.

716 [33] Capobianco M., Marelli S., *"Experimental investigation into the pulsating flow performance of a*
717 *turbocharger turbine in the closed and open waste-gate region"*, Proceedings of 9th
718 International Conference on Turbochargers and Turbocharging, p. 373-386, ISBN:
719 9781907599156, doi: 10.1243/17547164C0012010030, 2010.

720 [34] AVL BOOST v2011.2 Official Examples Library.

721 [35] Woschni G., *"A Universally Applicable Equation for the Instantaneous Heat Transfer*
722 *Coefficient in Internal Combustion Engines"*, SAE Paper 6700931

723 [36] K. Bayindir, M. et alii, "A comprehensive overview of hybrid electric vehicle: Powertrain
724 configurations, powertrain control techniques and electronic control units", Energy Conversion
725 and Management 52 (2011), 1305-1313.

726 [37] K.T. Chau, Y.S. Wong, "Overview of power management in hybrid electric vehicles", Energy
727 Conversion and Management 43 (2002), 1953-1968.

728 [38] 3DS Modelon official site: http://www.3ds.com/products/catia/portfolio/dymola

729 [39] Modelica official site: https://modelica.org/

730 [40] Frigo S., Pasini G., Marelli S., Lutzemberger G. et al., *"Numerical Evaluation of an Electric*
731 *Turbo Compound for SI Engines"* SAE Technical Paper 2014-32-0013, 2014,
732 doi:10.4271/2014-32-0013.

733 [41] G. Kouroussis, P. Dehombreux, O. Verlinden, "Vehicle and powertrain dynamics analysis with
734 an automatic gearbox", Mechanism and Machine Theory 83 (2015), 109-124.

735 [42] Modelica Libraries official site: https://modelica.org/libraries

736 [43] C. Lv, J. Zhang, Y.Li, Y. Yuan, "Mechanism analysis and evaluation methodology of
737 regenerative braking contribution to energy efficiency improvement of electrified vehicles",
738 Energy Conversion and Management 92 (2015), 469-482.

739 [44] BMW official site: http://www.bmw.com/com/en/insights/technology/technology_guide/articles/
740 mm_brake_energy_regeneration.html

741 [45] Common Artemis Driving Cycle (CADC) site: http://www.dieselnet.com/standards/cycles/
742 artemis.php

743 [46] Simpkin R., D'Ambrosio C., Simonsson J. et al., Energy Efficient Vehicles for Road Transport,
744 Transport Research Arena – Europe 2012, Athens (Greece), 23-26/4/2012.

745

746